

Parallel-Chain Monte Carlo Based on Generative Neural Networks

Hongyu Lu,¹ Chuhao Li,^{2,3} Wei Li,^{4,5,*} Yang Qi,^{6,7,†} and Zi Yang Meng^{1,‡}

¹*Department of Physics and HKU-UCAS Joint Institute of Theoretical and Computational Physics, The University of Hong Kong, Pokfulam Road, Hong Kong SAR, China*

²*Beijing National Laboratory for Condensed Matter Physics and Institute of Physics, Chinese Academy of Sciences, Beijing 100190, China*

³*School of Physical Sciences, University of Chinese Academy of Sciences, Beijing 100190, China*

⁴*Institute of Theoretical Physics, Chinese Academy of Sciences, Beijing 100190, China*

⁵*School of Physics, Beihang University, Beijing 100191, China*

⁶*State Key Laboratory of Surface Physics, Fudan University, Shanghai 200438, China*

⁷*Center for Field Theory and Particle Physics, Department of Physics, Fudan University, Shanghai 200433, China*

(Dated: August 17, 2021)

We design generative neural networks that generate Monte Carlo configurations with complete absence of autocorrelation and from which direct measurements of physical observables can be employed, irrespective of the system locating at the classical critical point, fermionic Mott insulator, Dirac semimetal and quantum critical point. We further propose a generic parallel-chain Monte Carlo scheme based on such neural networks, which provides independent samplings and accelerates the Monte Carlo simulations by reducing the thermalization process. We demonstrate the performance of our approach on the two-dimensional Ising and fermion Hubbard models.

Introduction — Monte Carlo (MC) method is a widely used numerical method to investigate problems in statistical physics and quantum many-body systems. Although its complexity is generally polynomial when the sign problem is absent, the complexity can still be prohibitively high for certain quantum problems. In particular, quantum Monte Carlo simulations of generic interacting-fermion systems [1–5], such as Hubbard model for correlated electrons [2, 3], Holstein model for electron-phonon interaction [6, 7], and the spin-fermion model of non-Fermi-liquid [5, 8, 9], to name a few, have very high complexity that scales at least to $\sim \beta N^3$ where $\beta = 1/T$ is the inverse temperature and the $N = L^d$ the total site number for a lattice model in d -dimension (such type of Monte Carlo is termed as determinant quantum Monte Carlo (DQMC) where the complexity comes from the matrix operation on the fermion determinant). The situation worsens when one wants to study critical points like the novel quantum critical points ubiquitously present in the metal-insulator transition, pseudogap and non-Fermi-liquids, and dynamics and transport properties in high-temperature superconductivity, etc. This can largely be ascribed to that the widely-used Markov-chain Monte Carlo (MCMC) method with local updates (or the Metropolis algorithm) suffers from very long Markov-chain autocorrelation (scales with the system size to a high power) due to the critical slowing down.

Although there exist powerful and highly efficient cluster/loop update scheme for classical problems such as the Ising model [10, 11] and quantum spin/boson systems such as Heisenberg and Bose-Hubbard models [12–15], such ingeniously designed algorithms do not exist for generic quantum many-body problems, especially for interacting-fermion systems, for example in DQMC. Therefore, the efforts for more efficient algorithms that could overcome these difficulties and boost the (quantum) Monte Carlo simulations for the aforementioned systems are called for.

In recent years, the application of Machine Learning tech-

nique has achieved notable success in physical systems ranging from statistical physics to condensed matter and quantum materials research [16–30]. The previous attempts of learning effective low-energy Hamiltonian that could help with accelerating the (quantum) MC sampling process, dubbed self-learning Monte Carlo scheme have shown the power of ideas from machine learning in improving the MC simulations of interacting fermion systems and inspired many extensions [8, 9, 31–42], but are still technically limited and have not enjoyed the developments of neural networks. On the other hand, studies of (generative) neural network models have shown interesting results such as normalizing flows[43–45], autoregressive models[46–48], etc. and some networks have been successfully applied to assist MC simulations [49–53].

Inspired by these developments, we design generative neural networks to approximate the distribution of MC configurations, and find the networks can be directly sampled with complete absence of autocorrelation. We demonstrate the powerful fitting ability of the neural networks by successfully generating configurations from which the correct physical observables can be directly measured for both classical $d = 2$ Ising model and quantum critical point of $d = 2$ fermion Hubbard model. In particular, the latter cannot be mapped to a classical model with short-range interactions due to the existence of gapless Dirac fermions, but it can still be successfully captured by the network. This suggests our approach can be applied to generic quantum systems including interacting fermionic models.

Moreover, we design a generic parallel-chain Monte Carlo (PCMC) scheme with the assistance of such neural networks, which “heals” the initial bias due to the unthermalized training set of the neural networks and provides very accurate results. We find the PCMC scheme with independent samplings can accelerate simulations especially in systems with long autocorrelation time by reducing the thermalization times and long measurement processes due to autocorrelation in traditional MCMC.

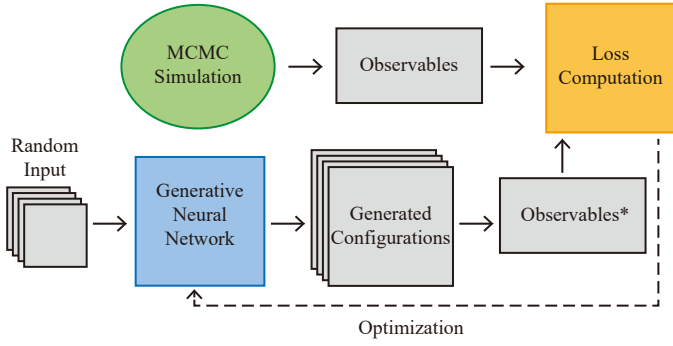


FIG. 1. Flow diagram for training the generative neural networks in this paper. The terms are as explained in the main text and the loss functions are defined in Eqs. (2) and (4), respectively.

Models — In this work, we aim to train neural networks to generate MC configurations that approach the distribution of the original Hamiltonian using convolutional and transposed convolutional architectures. Referring to the idea of the Generator in Generative Adversarial Nets (GAN) [54], we use random configurations (each element of the configurations is randomly set to be ± 1 with equal possibility) as input, which, after operations inside the networks, turn into the output of MC configurations distributed according to the physical Hamiltonian. The difference of our approach from GAN is that we do not need to build any Discriminator, but directly compare the physical observables, like the internal energy and magnetization (or magnetic structure factor) measured from output configurations of neural network with those obtained from MC simulations to optimize the parameters inside neural networks, as demonstrated in the flow diagram for training in Fig.1.

For the 2d square lattice Ising model:

$$H = -J \sum_{\langle i,j \rangle} \sigma_i \sigma_j \quad (1)$$

we study the system at the critical point ($T_c \approx 2.269$) with system sizes of 16×16 and 32×32 . We design the loss function directly related to the physical observables, i.e.,

$$\begin{aligned} Loss(\mathbf{G}_i, M_i, E_i) = & w_1 \sum_i [|M|(\mathbf{G}_i) - |M_i|]^2 \\ & + w_2 [M^2(\mathbf{G}_i) - M_i^2]^2 + w_3 [E(\mathbf{G}_i) - E_i]^2 \end{aligned} \quad (2)$$

where \mathbf{G} is the generated configuration, M refers to the magnetization $\frac{1}{N} |\sum_i \sigma_i|$, E refers to the energy density $\frac{1}{N} \langle H \rangle$ of the Ising system, and w_1 , w_2 , and w_3 are constants to balance each part of the loss.

For the 2d Hubbard model:

$$H = -t \sum_{\langle i,j \rangle, \sigma} (c_{i,\sigma}^\dagger c_{j,\sigma} + h.c.) + U \sum_i (n_{i,\uparrow} - \frac{1}{2})(n_{i,\downarrow} - \frac{1}{2}) \quad (3)$$

we consider the half-filled honeycomb lattices where it experiences a chiral Heisenberg Gross-Neveu quantum critical point at $U_c/t \approx 3.83$ between the Dirac semimetal and the

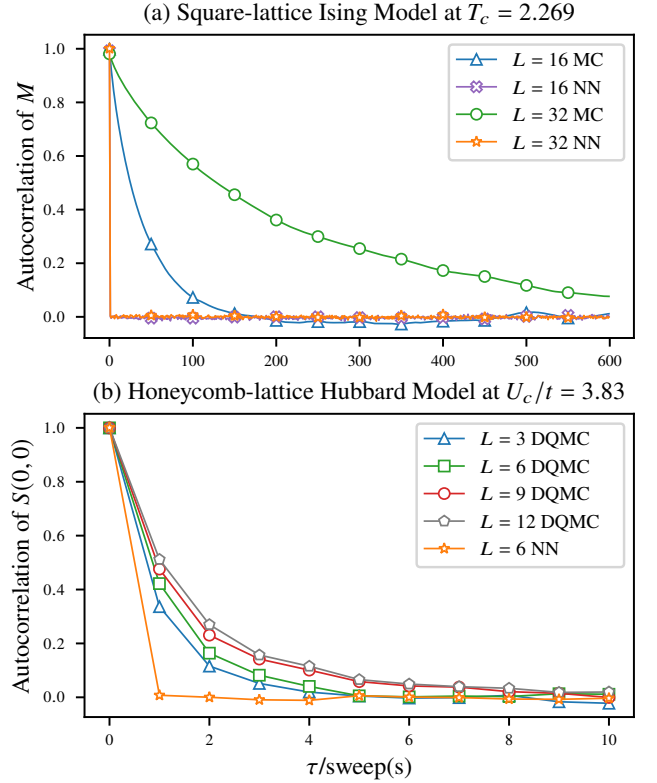


FIG. 2. Comparison of autocorrelation functions (here NN represents configurations generated from neural networks and (DQMC refers to samplings from Markov chains). (a) shows the autocorrelation of magnetization M for 2d Ising model from both MCMC and NN generated results at critical point $T_c = 2.269$ for $L = 16, 32$. The MC results exhibit the typical critical slowing down whereas the NN results have zero autocorrelation, i.e., direct *i.i.d.* sampling. (b) shows the autocorrelation for $S(0,0)$ of Hubbard model on honeycomb lattice at the Gross-Neveu QCP ($U_c/t = 3.83$) from DQMC with $L = 3, 6, 9, 12$, the critical slowing down manifest. The NN results again show no sign of autocorrelation.

antiferromagnetic Mott insulator [55–59]. Here the configuration is made of the auxiliary fields used in the discrete Hubbard-Stratonovich transformation to decouple the fermion interaction terms in DQMC, so the configurational space is of the size $L \times L \times \beta$ (see detailed explanation in Sec. I of Supplemental Materials (SM) [60]). We then design the loss function as:

$$Loss(\mathbf{G}_i, S_i, E_{k_i}) = w_1 \sum_i [S(\mathbf{G}_i) - S_i]^2 + w_2 \sum_i [E_k(\mathbf{G}_i) - E_{k_i}]^2, \quad (4)$$

where \mathbf{G} is the generated configuration, S refers to the structure factor $S(\mathbf{Q}) = \frac{1}{N} \sum_{ij} e^{-i\mathbf{Q} \cdot (\mathbf{r}_i - \mathbf{r}_j)} \langle s_i^z s_j^z \rangle$ ($s_i^z = \frac{1}{2}(n_{i,\uparrow} - n_{i,\downarrow})$) and $S(\Gamma = (0,0))$ is chosen for honeycomb lattice here, and E_k is the kinetic energy $\frac{1}{N} \sum_{\langle i,j \rangle, \sigma} \langle (c_{i,\sigma}^\dagger c_{j,\sigma} + h.c.) \rangle$, with constants w_1 and w_2 .

Our networks are all based on Tensorflow [61], and we complement with more details of the Ising and Hubbard models in Sec.I and those of neural networks in Sec.II of SM [60].

Autocorrelation analysis — In MCMC, the autocorrelation time, associated with the particular update scheme, can be extremely long in the physically interesting parameter regime like, e.g., near the classical and quantum critical points. And it is even worse when one performs the finite size analysis as the autocorrelation time usually increase with system size with a high power [10, 33, 40]. It therefore benefits a lot that the independent and direct samplings from the neural networks are completely free of autocorrelation. We demonstrate these behaviors quantitatively by measuring the autocorrelation function (defined in Sec.I.3 of SM [60]) of magnetization for 2d Ising model at $T_c = 2.269$ in Fig. 2(a), and of $S(0, 0)$ for the honeycomb-lattice Hubbard model at the Gross-Neveu QCP ($U_c/t = 3.83$) in Fig. 2(b), between the results generated by neural networks and MCMC results. It can be observed that, for the MCMC the autocorrelation functions decay slowly in Monte Carlo steps and the autocorrelation time for classical (quantum) critical points increases with the system size, but in results from neural networks, such autocorrelation has been completely eliminated.

PCMC algorithm based on neural networks — We now introduce the PCMC algorithm. In order to demonstrate its ability of correcting the error in the training sample, we no longer train the networks to approximate well-thermalized MC results, but take unthermalized MC configurations generated from short Markov chains. After training the neural networks and generate independent configurations, we add parallel MC updates starting from these generated configurations [62] and find the PCMC results quickly converge to the well-thermalized results. The whole process is summarized in Alg. 1.

Algorithm 1: PCMC scheme based on neural networks

- 1: Run a short Markov-chain(unthermalized) as training samples
 - 2: Train a generative neural network using observables from training samples
 - 3: Generate configurations from the trained neural network
 - 4: Start short MC steps from the generated *i.i.d.* configurations and make measurements
-

Numerical experiments on the Ising model — In the standard MCMC, the Markov chains must first be well thermalized such that it converges to the correct distribution, and then generate enough bins of statistically uncorrelated configurations to yield expectation values of observables with satisfactory statistical error, which requires the thermalization and each bin to be longer than the system-size-dependent autocorrelation time. To demonstrate that PCMC largely reduces the thermalization process, we compare the performance of PCMC on 16×16 Ising model at critical point, with those starting parallel MCMC simulations from random configurations and configurations used as training samples in PCMC, by computing the MC sweeps needed for converged magnetization results ($M^* = 0.713$ for $L = 16$ and $T = T_c$ as reference). We run 50 iterations for all three sets of data with each set consisting of

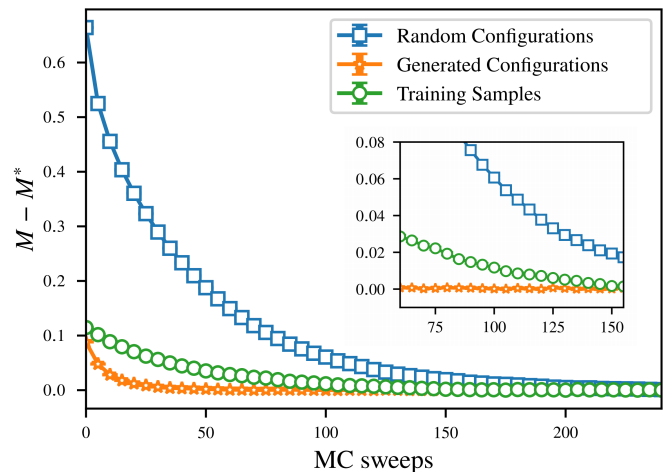


FIG. 3. Comparing the convergence time of magnetization (MC sweeps needed to converge) between PCMC and the two MCMC simulations of random configurations and configurations used for training the neural network, respectively. We set $M^* = 0.713$ for reference. For all three sets (each consisted of 1000 configurations), we run 50 iterations from the beginning to derive the expectations with standard errors. The inset further highlight the superiority of PCMC and the scale on y-axis is not changed.

1000 configurations, and the results are shown in Fig. 3. For training samples, almost about 150 sweeps are needed to reach a convergence, and for random configurations the number is more than 200. Remarkably, the PCMC scheme greatly lowers the thermalization time and arrive at the convergence after about only 30 sweeps.

To further quantify the comparison, we take the training part for neural networks into consideration, and compute on the same CPU that for the 150 epochs of network training that are more than sufficient to converge the hyper parameters in the neural network, it takes around 125 seconds (could be made even faster on GPU), and each MC sweep for 1000 configurations takes around 2.5 seconds. That is, PCMC takes $125 + 2.5 * 30 = 200$ seconds for the 1000 thermalized and independent configurations here from training samples, while the 1000 samples themselves need up to $2.5 * 150 = 375$ seconds for thermalization. Therefore, we claim that PCMC can overall speed up the MC simulations. Besides, the independent PCMC samples also save time in the process of measurements as there is completely no autocorrelation and we can directly measure observables once the thermalization is completed.

Metric	MC Train	NN	PCMC	Good MC
$ M $	0.600(7)	0.606(3)	0.713(6)	0.713(3)
E	-1.373(6)	-1.329(4)	-1.454(5)	-1.453(2)

TABLE I. Numerical results of PCMC on square lattice Ising model ($L = 16$, $T_c = 2.269$). The four sets of data respectively refers to training samples (unthermalized), neural network generated results, PCMC results (30 MC sweeps), and well-thermalized MC results. Results shown here are expectations with standard errors from 1000 values (and good MC takes 1000 bins).

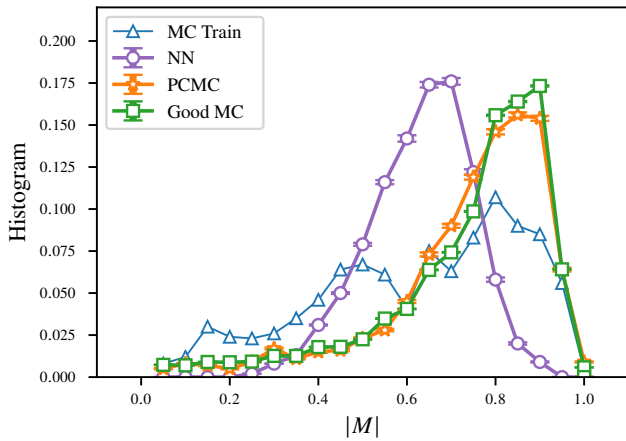


FIG. 4. Histograms of the distribution of magnetization and the abbreviations are the same as in Table.I. We obtain standard errors from 50 iterations of PCMC (30 MC sweeps and 1000 configurations each) in total with MC Train fixed, and the Good MC are from 50 sets (each set consists of 200000 values).

For better display, we then show the details of observables by taking 1000 configurations from the beginning of a rather short Markov-chain as training samples to run PCMC and the numerical results are shown in Table.I. We also plot the corresponding histograms of distribution of magnetization in Fig.4 after 50 iterations of PCMC (1000 configurations for each iteration) from the same training samples. The observables obtained from unthermalized training samples are far worse than those thermalized. After training, the neural network generates configurations with approximately the same observables but of Gaussian-like distributions. After we add 30 MC updates on the generated configurations, they quickly converge to the results of the so-called Good MC, which consists of totally 200000 well thermalized MC configurations for reference (we take 1000 bins with 200 configurations per bin). Moreover, the distribution of PCMC has a large overlap with Good MC. To quantitatively analyze the overlap of distribution, we compute the percentage overlap ($\%OL$) between two histograms [52], i.e., $\%OL(P_r, P_\theta) = \sum_i \min(P_r(i), P_\theta(i))$, where P_r and P_θ corresponds to the distributions to be compared and we divide them into 20 bins. Again we count the PCMC samples from 50 iterations for statistical expectation with standard error. The result is $\%OL = 94.78(18)$, which reconfirms that the distribution of PCMC with just 1000 configurations has a large overlap with that of Good MC.

Metric	DQMC Train	PCMC	Good DQMC
E_k	-1.360(4)	-1.357(3)	-1.358(1)
$S(\Gamma)$	3.11(10)	2.99(10)	3.00(4)

TABLE II. Numerical results of PCMC on honeycomb lattice Hubbard model at ($U_c/t = 3.83, L = 6$). The three sets of data respectively refers to training samples (unthermalized), PCMC results, and well-thermalized DQMC results. Results shown here are expectations with standard errors from 1000 values(Good DQMC take 1000 bins).

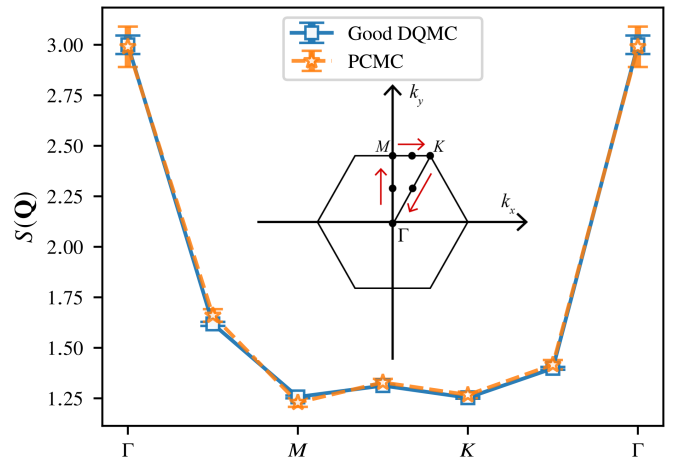


FIG. 5. Comparison of magnetic structure factor $S(\mathbf{Q})$ between Good DQMC (10000 samples) and PCMC (15 sweeps), which are not used for network training except $S(\Gamma)$. The black dots in the inset are the momenta measured along the high-symmetry path (with red arrows).

Hubbard model on the honeycomb lattice — Beyond classical Ising model, we take 2d Hubbard model on honeycomb lattice at its unique Gross-Neveu quantum criticality ($U_c/t = 3.83, L = 6$) as an example of interacting fermion systems. We run PCMC with 15 DQMC sweeps from 1000 generated configurations and the mean values with errorbars of physical observables are listed in Tab. II. The PCMC results again present almost identical expectation values of physical observables as the Good DQMC (consisting of 10000 configurations in total and divided into 1000 bins). Furthermore, in Fig. 5 we show the magnetic structure $S(\mathbf{Q})$ along the high-symmetry path of the Brillouin zone, which are observables not used in training the networks. We find the agreements between PCMC and good MC are perfect, only after 15 sweeps in PCMC. These results confirm the neural networks with optimizers like Adam [63] are capable of fixing the large-scale determinant computations. We have to clarify that in PCMC we do not necessarily need up to 1000 configurations (as we use for example here), which can further reduce the computational burden.

Discussion — We develop PCMC scheme based on the generative neural networks. Our numerical results support firmly that the generative neural networks as independent and direct samplings can approximately capture the distribution of MC configurations and completely get rid of autocorrelation in the study of classical and quantum many-body systems. Furthermore, PCMC provides a generic scheme for speeding up the MC simulations by reducing the thermalization time and saving time for direct measurement of observables from those independent PCMC samples.

From the perspective of neural networks, we verify that simulations of interacting fermion systems, such as DQMC, can be merged into the loss function of neural networks. The next step from here is to use generative neural networks to provide efficient and accurate system-size extrapolations of MC configurations and in this way, many more complex yet

fundamental problems, such as the twisted bilayer graphene and quantum Moiré materials, where the DQMC has just been shown to be able to solve the lattice models [64–68] but with heavy computational costs, could be improved in PCMC.

Acknowledgments — We thank Zheng Yan, Shangqiang Ning, Bin-bin Mao, Jiarui Zhao, Chengkang Zhou, and Xu Zhang for the enjoyable discussions and happy conversations in the No. 16 Pavillion of Lung Fu Shan Country Park. We acknowledge support from the RGC of Hong Kong SAR of China (Grant Nos. 17303019, 17301420 and AoE/P-701/20), NSFC (Grant Nos. 11974036, 11874115 and 11834014), and the Strategic Priority Research Program of the Chinese Academy of Sciences (Grant No. XDB33000000). We thank the Center for Quantum Simulation Sciences in the Institute of Physics, Chinese Academy of Sciences, the Computational Initiative at the Faculty of Science and the Information Technology Services at the University of Hong Kong for their technical support and generous allocation of GPU/CPU time. This work is also supported by the Seed Funding "Quantum-Inspired explainable-AI" at the HKU-TCL Joint Research Centre for Artificial Intelligence, Hong Kong.

* w.li@itp.ac.cn

† qiyang@fudan.edu.cn

‡ zymeng@hku.hk

- [1] R. Blankenbecler, D. J. Scalapino, and R. L. Sugar, *Phys. Rev. D* **24**, 2278 (1981).
- [2] J. E. Hirsch, *Phys. Rev. B* **28**, 4059 (1983).
- [3] J. E. Hirsch, *Phys. Rev. B* **31**, 4403 (1985).
- [4] F. Assaad and H. Evertz, World-line and determinantal quantum monte carlo methods for spins, phonons and electrons, in *Computational Many-Particle Physics*, edited by H. Fehske, R. Schneider, and A. Weiße (Springer Berlin Heidelberg, Berlin, Heidelberg, 2008) pp. 277–356.
- [5] X. Y. Xu, Z. H. Liu, G. Pan, Y. Qi, K. Sun, and Z. Y. Meng, *Journal of Physics: Condensed Matter* **31**, 463001 (2019).
- [6] R. T. Scalettar, N. E. Bickers, and D. J. Scalapino, *Phys. Rev. B* **40**, 197 (1989).
- [7] R. M. Noack, D. J. Scalapino, and R. T. Scalettar, *Phys. Rev. Lett.* **66**, 778 (1991).
- [8] X. Y. Xu, K. Sun, Y. Schattner, E. Berg, and Z. Y. Meng, *Phys. Rev. X* **7**, 031058 (2017).
- [9] Z. H. Liu, G. Pan, X. Y. Xu, K. Sun, and Z. Y. Meng, *Proceedings of the National Academy of Sciences* **116**, 16760 (2019).
- [10] R. H. Swendsen and J.-S. Wang, *Phys. Rev. Lett.* **58**, 86 (1987).
- [11] U. Wolff, *Phys. Rev. Lett.* **62**, 361 (1989).
- [12] A. W. Sandvik, *Phys. Rev. B* **59**, R14157 (1999).
- [13] N. V. Prokof'ev, B. V. Svistunov, and I. S. Tupitsyn, *J. Exp. Theor. Phys.* **87**, 310 (1998).
- [14] N. V. Prokof'ev, B. V. Svistunov, and I. S. Tupitsyn, *Phys. Lett. A* **238**, 253 (1998).
- [15] A. W. Sandvik, *AIP Conference Proceedings* **1297**, 135 (2010), <https://aip.scitation.org/doi/pdf/10.1063/1.3518900>.
- [16] G. Carleo, I. Cirac, K. Cranmer, L. Daudet, M. Schuld, N. Tishby, L. Vogt-Maranto, and L. Zdeborová, *Rev. Mod. Phys.* **91**, 045002 (2019).
- [17] J. Carrasquilla, *Advances in Physics: X* **5**, 1797528 (2020).
- [18] E. Bedolla, L. C. Padierna, and R. Castañeda-Priego, *Journal of Physics: Condensed Matter* **33**, 053001 (2020).
- [19] K. Ch'ng, J. Carrasquilla, R. G. Melko, and E. Khatami, *Phys. Rev. X* **7**, 031038 (2017).
- [20] P. Broecker, J. Carrasquilla, R. G. Melko, and S. Trebst, *Scientific Reports* **7**, 8823 (2017).
- [21] J. Carrasquilla and R. G. Melko, *Nature Physics* **10.1038/nphys4035** (2017).
- [22] G. Carleo, Y. Nomura, and M. Imada, *Nature Communications* **10.1038/s41467-018-07520-3** (2018).
- [23] G. Carleo and M. Troyer, *Science* **355**, 602 (2017).
- [24] Z. Cai and J. Liu, *Phys. Rev. B* **97**, 035116 (2018).
- [25] K. Choo, G. Carleo, N. Regnault, and T. Neupert, *Phys. Rev. Lett.* **121**, 167204 (2018).
- [26] S. Cheng, L. Wang, T. Xiang, and P. Zhang, *Phys. Rev. B* **99**, 155131 (2019).
- [27] C. Guo, Z. Jie, W. Lu, and D. Poletti, *Phys. Rev. E* **98**, 042114 (2018).
- [28] Z.-Y. Han, J. Wang, H. Fan, L. Wang, and P. Zhang, *Phys. Rev. X* **8**, 031012 (2018).
- [29] H. Xie, L. Zhang, and L. Wang, (2021), [arXiv:2105.08644 \[cond-mat.str-el\]](https://arxiv.org/abs/2105.08644).
- [30] S. Efthymiou, M. J. S. Beach, and R. G. Melko, *Phys. Rev. B* **99**, 075113 (2019).
- [31] J. Liu, Y. Qi, Z. Y. Meng, and L. Fu, *Phys. Rev. B* **95**, 041101(R) (2017).
- [32] J. Liu, H. Shen, Y. Qi, Z. Y. Meng, and L. Fu, *Phys. Rev. B* **95**, 241104(R) (2017).
- [33] X. Y. Xu, Y. Qi, J. Liu, L. Fu, and Z. Y. Meng, *Phys. Rev. B* **96**, 041119(R) (2017).
- [34] Y. Nagai, H. Shen, Y. Qi, J. Liu, and L. Fu, *Phys. Rev. B* **96**, 161102(R) (2017).
- [35] L. Huang and L. Wang, *Phys. Rev. B* **95**, 035105 (2017).
- [36] L. Huang, Y.-f. Yang, and L. Wang, *Phys. Rev. E* **95**, 031301(R) (2017).
- [37] K. Endo, T. Nakamura, K. Fujii, and N. Yamamoto, *Phys. Rev. Research* **2**, 043442 (2020).
- [38] Z. H. Liu, X. Y. Xu, Y. Qi, K. Sun, and Z. Y. Meng, *Phys. Rev. B* **98**, 045116 (2018).
- [39] Z. H. Liu, X. Y. Xu, Y. Qi, K. Sun, and Z. Y. Meng, *Phys. Rev. B* **99**, 085114 (2019).
- [40] C. Chen, X. Y. Xu, J. Liu, G. Batrouni, R. Scalettar, and Z. Y. Meng, *Phys. Rev. B* **98**, 041102(R) (2018).
- [41] C. Chen, X. Y. Xu, Z. Y. Meng, and M. Hohenadler, *Phys. Rev. Lett.* **122**, 077601 (2019).
- [42] W. Jiang, Y. Liu, A. Klein, Y. Wang, K. Sun, A. V. Chubukov, and Z. Y. Meng, [arXiv:2105.03639](https://arxiv.org/abs/2105.03639).
- [43] L. Zhang, W. E, and L. Wang, (2018), [arXiv:1809.10188 \[cs.LG\]](https://arxiv.org/abs/1809.10188).
- [44] G. S. Hartnett and M. Mohseni, (2020), [arXiv:2001.00585 \[cs.LG\]](https://arxiv.org/abs/2001.00585).
- [45] S.-H. Li and L. Wang, *Phys. Rev. Lett.* **121**, 260601 (2018).
- [46] D. Wu, L. Wang, and P. Zhang, *Phys. Rev. Lett.* **122**, 080602 (2019).
- [47] O. Sharif, Y. Levine, N. Wies, G. Carleo, and A. Shashua, *Phys. Rev. Lett.* **124**, 020503 (2020).
- [48] J.-G. Liu, L. Mao, P. Zhang, and L. Wang, *Machine Learning: Science and Technology* **2**, 025011 (2021).
- [49] D. Alcalde Puente and I. M. Eremin, *Phys. Rev. B* **102**, 195148 (2020).
- [50] M. S. Albergó, G. Kanwar, and P. E. Shanahan, *Phys. Rev. D* **100**, 034515 (2019).
- [51] B. McNaughton, M. V. Milošević, A. Perali, and S. Pilati, *Phys. Rev. E* **101**, 053312 (2020).

- [52] J. Singh, V. Arora, V. Gupta, and M. S. Scheurer, (2020), arXiv:2006.11868 [cond-mat.stat-mech].
- [53] D. Wu, R. Rossi, and G. Carleo, arXiv e-prints , arXiv:2105.05650 (2021), arXiv:2105.05650 [cond-mat.stat-mech].
- [54] I. J. Goodfellow *et al.*, *Proceedings of the 27th International Conference on Neural Information Processing Systems - Volume 2, NIPS'14*, 2672–2680 (2014).
- [55] Z. Y. Meng, T. C. Lang, S. Wessel, F. F. Assaad, and A. Muramatsu, *Nature* **464**, 847 (2010).
- [56] S. Sorella, Y. Otsuka, and S. Yunoki, *Scientific Reports* **2**, 992 (2012).
- [57] F. F. Assaad and I. F. Herbut, *Phys. Rev. X* **3**, 031010 (2013).
- [58] T. C. Lang and A. M. Läuchli, *Phys. Rev. Lett.* **123**, 137602 (2019).
- [59] Y. Liu, W. Wang, K. Sun, and Z. Y. Meng, *Phys. Rev. B* **101**, 064308 (2020).
- [60] Detailed description of lattice models, determinantal quantum Monte Carlo for fermion Hubbard model and architecture and optimization of neural networks.
- [61] M. Abadi *et al.*, arXiv e-prints , arXiv:1603.04467 (2016), arXiv:1603.04467 [cs.DC].
- [62] For direct measurement on the generated configurations, we map each generated number from the range of (0, 1) to (-1, 1) and the relationship is: number for measurement = generated number * 2 - 1. For MC update, we use Bernoulli distribution to discretize each element with the initial generated number as the possibility to take the value 1, and map every 0 to -1.
- [63] D. P. Kingma and J. Ba, *3rd International Conference on Learning Representations, Conference Track Proceedings*, (2015).
- [64] X. Zhang, G. Pan, Y. Zhang, J. Kang, and Z. Y. Meng, *Chinese Physics Letters* **38**, 077305 (2021).
- [65] Y.-D. Liao, X.-Y. Xu, Z.-Y. Meng, and J. Kang, *Chinese Physics B* **30**, 017305 (2021).
- [66] J. S. Hofmann, E. Khalaf, A. Vishwanath, E. Berg, and J. Y. Lee, arXiv e-prints , arXiv:2105.12112 (2021), arXiv:2105.12112 [cond-mat.str-el].
- [67] Y. D. Liao, J. Kang, C. N. Breiø, X. Y. Xu, H.-Q. Wu, B. M. Andersen, R. M. Fernandes, and Z. Y. Meng, *Phys. Rev. X* **11**, 011014 (2021).
- [68] Y. DaLiao, Z. Y. Meng, and X. Y. Xu, *Phys. Rev. Lett.* **123**, 157601 (2019).

SUPPLEMENTAL MATERIAL

PHYSICAL MODELS

1. Model Details

First we consider two-dimensional Ising model on square lattice at the critical point $T_c \approx 2.269$ and the Hamiltonian is shown in Eq.(1) of the main text, which can be solved with classical Monte Carlo simulations. σ_i and σ_j refers to nearest neighbors of classical spins and take values: ± 1 . We set the interaction strength J of all pairs of neighbors to be 1.

Next, we consider Hubbard model on the honeycomb lattice, which can be solved with determinant quantum Monte Carlo (DQMC) at half-filling. In Eq.(3) of main text, t is the hopping parameter for the kinetic energy, U is the repulsive Coulomb interaction between electrons on the same lattice site, $\langle i, j \rangle$ represents a pair of nearest-neighbor sites in the lattice, the operators $c_{i,\sigma}^\dagger$ and $c_{i,\sigma}$ are the fermion creation and annihilation operators for fermions with z component of spin-up ($\sigma = \uparrow$) or spin-down ($\sigma = \downarrow$), and the operators $n_{i,\sigma} = c_{i,\sigma}^\dagger c_{i,\sigma}$ are the number operators which count numbers of fermions of spin σ on the site i . In loss function Eq.(4) in the main text, S refers to the structure factor: $S(\mathbf{Q}) = \frac{1}{L^2} \sum_{ij} e^{-i\mathbf{Q}\cdot(\mathbf{r}_i-\mathbf{r}_j)} \langle s_i^z s_j^z \rangle$, and the spin operator $\mathbf{s}_i = \frac{1}{2} \sum_{\alpha\alpha'} c_{i,\alpha}^\dagger \vec{\sigma}_{\alpha\alpha'} c_{i,\alpha'}$. Note here $\vec{\sigma}$ denotes the Pauli matrices and so the z -component $s_i^z = \frac{1}{2}(n_{i\uparrow} - n_{i\downarrow})$.

2. Determinant Quantum Monte Carlo (DQMC)

The partition function $Z = \text{Tr}\{e^{-\beta H}\}$ is expressed as a path integral by discretizing the inverse temperature β into L_τ slices of length $\Delta\tau$. Then, after Trotter-Suzuki decomposition, the Hamiltonian are separated in each time slice and Z can be written as

$$Z = \text{Tr} \left[\prod_{l=1}^{L_\tau} e^{-\Delta\tau H_k} e^{-\Delta\tau H_U} \right] + O(\Delta\tau^2), \quad (\text{S1})$$

where $H_k = -t \sum_{\langle i,j \rangle, \sigma} (c_{i,\sigma}^\dagger c_{j,\sigma} + h.c.)$ is the kinetic term and $H_U = U \sum_i (n_{i,\uparrow} - \frac{1}{2})(n_{i,\downarrow} - \frac{1}{2})$ is interaction term of the Hubbard model.

To treat the quartic interaction term, the discrete Hubbard-Stratonovich transformation[1-3] can be applied and then $e^{-\Delta\tau H_U} = e^{-U\Delta\tau(n_{i,\uparrow}-\frac{1}{2})(n_{i,\downarrow}-\frac{1}{2})} = \frac{1}{2} e^{-\frac{U\Delta\tau}{4}} \sum_{S_i=\pm 1} e^{\nu S_i(n_{i,\uparrow}-n_{i,\downarrow})}$, where the scalar ν is defined by $\cosh \nu = e^{\frac{U\Delta\tau}{2}}$. Putting kinetic part and interaction part together, the term in partition function becomes

$$e^{-\Delta\tau H_k} e^{-\Delta\tau H_U} = \prod_{\sigma} e^{-\Delta\tau T_{\sigma}} e^{\sigma \nu S_i n_{i,\sigma}}, \quad (\text{S2})$$

where H_k is rewritten with operator $T_\sigma = -t \sum_{i,j} c_{i,\sigma}^\dagger c_{j,\sigma} + h.c..$ According to the feature of fermion operator[1], a fermion operator (\hat{M}_l for example) with a quadratic form like $\hat{M}_l = \sum_{i,j} c_i^\dagger (M_l)_{ij} c_j$ satisfies

$$\text{Tr} \left[e^{-\hat{M}_1} e^{-\hat{M}_2} \dots e^{-\hat{M}_L} \right] = \text{Det} [I + e^{-M_1} e^{-M_2} \dots e^{-M_L}]. \quad (\text{S3})$$

Then the partition function could be finally written in determinant form as

$$Z = \left(\frac{1}{2} e^{-\frac{U\Delta\tau}{4}} \right)^{NL_\tau} \sum_{s_{i,l}} \prod_{\sigma} \text{Det} [I + B^\sigma(L_\tau, L_\tau - 1) \dots B^\sigma(1, 0)], \quad (\text{S4})$$

in which

$$B^\sigma(l_2, l_1) = \prod_{l=l_1+1}^{l_2} e^{\sigma \nu \text{Diag}\{s_{i,l}\}} e^{-A\tau T}, \quad (\text{S5})$$

where $\sigma = \{1, -1\}$ in calculation corresponding mark $\{\uparrow, \downarrow\}$, and T is the matrix corresponding to the operator T_σ . Thus, we have introduced a sum over the field of auxiliary variables $s_{i,l}$ in a $(d+1)$ -dimension space (d for spatial denoted by i and 1 for imaginary time denoted by l) as shown in Fig. S1 (b), and the fermionic degrees of freedom in the quadratic form have been integrated out analytically. Note B^σ is an $N \times N$ matrix that depends on the auxiliary configurations.

3. Autocorrelation Function

The autocorrelation function for an observable O is defined as:

$$A_O(t) = \frac{\langle O(i+t)O(i) \rangle - \langle O \rangle^2}{\langle O^2 \rangle - \langle O \rangle^2}. \quad (\text{S6})$$

For MCMC, i and t denotes the simulation time, normally in units of the MC sweeps, and the averages are over the reference time i . For Neural Network results, when computing the formal autocorrelation function, i and t simply refers to the serial numbers of the configurations.

NEURAL NETWORK DETAILS

1. Architecture

For 2d Ising model on square lattice (16×16 for example), the network structure is shown in Fig. S1 (a). For the random input, we fix its shape to be the same as that of the Monte Carlo configurations. Inside the network, inspired by the network structure in Ref.[30], we use three 2d convolutional layers, with 64 filters of size 8×8 for the first layer, 32 filters of size 1 for the second, and 1 filter of size 6×6 for the third layer. We choose rectified linear function $\text{ReLU}(x) = \max(0, x)$ in the first and second convolutional layers and sigmoid function $\sigma(x) = 1/(1 + e^{-x})$ in the third. We also apply periodic boundary condition (PBC) layers each time before the convolutional layers if the kernel dimension is larger than one, which provides the configuration tensors with paddings of boundary elements instead of 0s (the padding size is decided by the size of filters in the corresponding convolutional layer, so as to ensure the shape invariance of the configuration tensors after convolutional operations).

In the case of 2d Hubbard model on the honeycomb lattice ($6 \times 6 \times 2$ for example), we switch from classical Ising configurations to the auxiliary field configurations of the DQMC[3,33], with the configuration space of $\beta \times L \times L \times 2$ where $\beta = 1/T$ is the inverse temperature. We set $\beta = 6$ and the Trotter discretization $\Delta\tau = 0.1$, so the DQMC auxiliary field configurations are of shape $60 \times 12 \times 6$ (note the 2 site per unit cell for the honeycomb lattice), as schematically shown in Fig. S1 (b). As shown in Eq.(4), we have to carry out large-scale determinant computation to measure the observables from generated configurations in order to compute the loss, and thus the complexity for the optimization is much larger than the case of classical model. Therefore, instead of the previous PBC-based network structure, we try another architecture of transposed convolutional layers and feed smaller random configurations as input. We find it is still capable of fitting the results we want and optimize faster. As shown in Fig. S1 (c) for the example model, we build two 3d transposed convolutional layers, with all filters using valid padding and sigmoid function as activation. There are 20 filters of size $16 \times 6 \times 3$ in the first layer and 1 filter of size $36 \times 6 \times 3$ in the second and the random input configurations are of shape $10 \times 2 \times 2$ while the predicted output are of shape $60 \times 12 \times 6$.

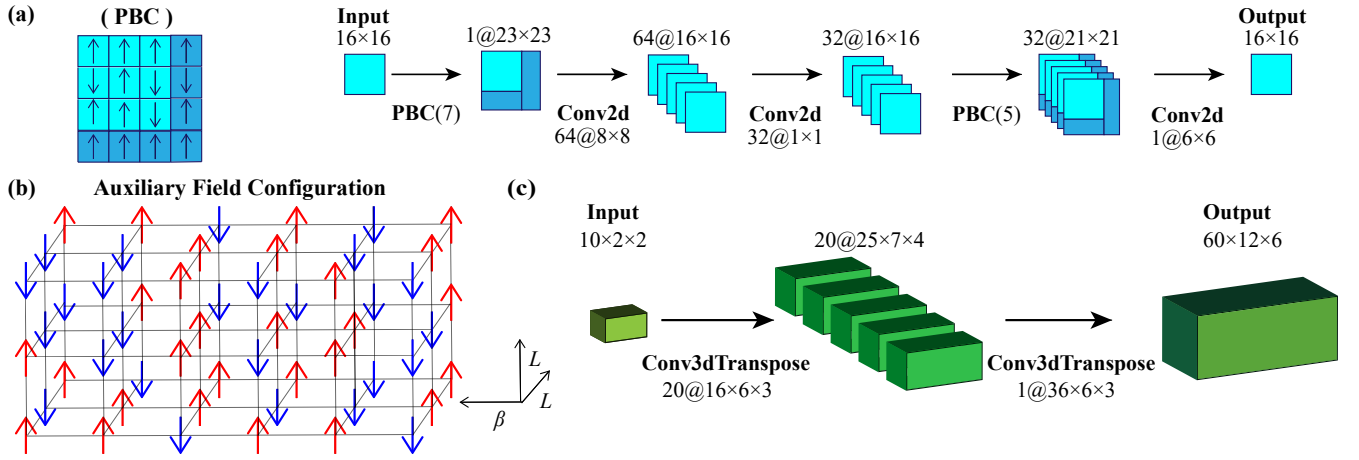


FIG. S1. Schematic figures for the generative neural networks used in this study. (a) shows an example of periodic boundary condition on the left, and we use the neural network structure on the right for the training of the 2d Ising model, where Conv2d stands for 2d convolutional layer. (b) displays the auxiliary field configuration in DQMC for the Hubbard model, with the $(2+1)d$ space-time of $\beta \times L \times L$. The auxiliary fields of ± 1 live on each space-time lattice site. (c) demonstrates the schematic structure of 3d transposed convolutional network we employed for the training of the 2d Hubbard model on $6 \times 6 \times 2$ honeycomb lattice.

2. Optimization

In order to optimize such neural networks, for both classical and quantum models, we prepare 1000 sets of observables measured from MC simulations and take 1000 input random configurations which will be processed into generated configurations. The comparison in loss function is randomly distributed without any grouping. For the choice of observables in the defined loss functions, we simply pick some from the ones we usually focus on. In the Ising case, we take the batch size to be 5 and epoch number to be up to 150 as the computation is quite easy. While in the Hubbard case, we run at most 15 epochs with a batch size of 3. We optimize the network parameters using Adam[63] with conventional learning rate 10^{-3} , $\beta_1 = 0.9$, and $\beta_2 = 0.999$.